(Received 17 June 2025, Accepted 27 August 2025, Scheduled 4 September 2025)

A Four Port Super-Wideband MIMO Antenna with Improved Inter-Port Isolation and Dual-Band Interference Suppression Capability

Chanprit Kaur[1], Raghvenda K. Singh[2,*], and Kiran K. Verma[1]

[1] *Department of Physics and Electronics*
Dr. Rammanohar Lohia Avadh University, Ayodhya 224001, Uttar Pradesh, India
[2] *Department of Electronics and Communication Engineering*
Jaypee Institute of Information Technology, Noida 201309, Uttar Pradesh, India

ABSTRACT: In this paper, a 4-port multiple input multiple output (MIMO) antenna with dual-notched bands and high interference rejection features is presented for ultra-wideband and beyond. The total volume of the intended antenna, computed at 2.63 GHz, is $0.52\lambda \times 0.52\lambda \times 0.014\lambda$. The basic radiating element consists of a spatula-shaped patch etched with a U and an inverted U-shaped slots printed on the top of a dielectric substrate, which is backed by defected partial ground plane. With the goal of achieving good polarization diversity and high isolation, four identical basic elements are arranged in orthogonal way to form the MIMO configuration. The inter-element isolation has been improved by a swastik-shaped decoupling structure with its arms extended in the form of meander-lines. As a result, the isolation between diagonal and orthogonal elements is better than 20 dB and 25 dB, respectively with envelope correlation coefficient < 0.012 and diversity gain > 9.995 dB. The suggested antenna attains an impedance bandwidth of 2.63–18.44 GHz with ability to shield interferences from 3.38–3.90 GHz and 4.65–6.45 GHz, specifically targeting frequencies associated with WLAN/ISM and Wi-MAX/LTE bands, respectively. Moreover, it exhibits maximum radiation efficiency and gain of 97.88% and 5.94 dBi, respectively in the working band.

1. INTRODUCTION

Of late, paradigm shifts in the wireless communication technology have given rise to ultra-wideband (UWB) antennas that can cover multiple applications at once, including internet-of-things (IoT), cognitive radio, sensing networks, medical field, low frequency smart devices, radar, and satellite systems [1–3]. UWB technology offers distinct advantages such as high data throughput, wide bandwidth, low power consumption, and inherent security feature [4]. However, UWB antenna systems inevitably interfere with signals from several existing narrowband short-range wireless technologies like LTE, WiMAX, WLAN, C-band, and X-band. Therefore, an antenna that can filter out a specific band falling in UWB range has attracted a lot of interest. In addition, UWB technology encounters issues like reflection and diffraction within the medium, leading to multipath fading and signal losses, thereby degrading end-to-end communication [5]. Addressing these challenges and in turn improving the channel capacity is crucial in contemporary wireless communication systems [6]. The integration of multiple input multiple output (MIMO) antenna systems equipped with high diversity performance and UWB technology has been proven to be an effective approach to suppress multipath fading, thus resulting in enhanced communication quality and channel capacity [7, 8]. However, MIMO antenna necessitates low correlation among the several antenna elements laid over the same substrate, especially in the devices operating within confined space [9, 10]. Various techniques have been reported in the literature to reduce mutual coupling among the radiating elements, viz., defected ground structure (DGS) [1], metamaterial (MTM) structure [11], neutralization lines [12], parasitic elements [13], electromagnetic band gap (EBG) structures [14], decoupling structure [15], and slots in the substrate [16] to name the few.

Modak et al. discussed two configurations of a 4×4 MIMO design with dual-band notch feature in the range of 3.1–10.8 GHz [17]. They were able to achieve very good isolation of 25 dB; however, the use of a couple of mushroom EBG structures to shield 6.3–7.76 GHz band poses fabrication challenge. In another approach, Chen et al. [13] studied a UWB-MIMO antenna with an impedance bandwidth (IBW) of 2.5–12 GHz with feature to reject 3.3–3.9 GHz WiMAX, 5–6 GHz WLAN, and 7.4–8.5 GHz X-bands. However, the usage of EBG (for notch) and shorted parasitic strips (to reduce inter-port correlation) makes the development of this antenna complex. In [15], the authors have presented a large 4-port MIMO configuration with isolation better than 20 dB, achieved using a fan-shaped parasitic decoupler. Further, another 4-port MIMO system utilized complex fractal MTM-EBG to achieve isolation greater than 17 dB in narrow band of 8–9.5 GHz [14]. A two-sided orthogonally connected 4×4 MIMO design

* Corresponding author: Raghvenda Kumar Singh (raghvenda.singh@jiit.ac.in).

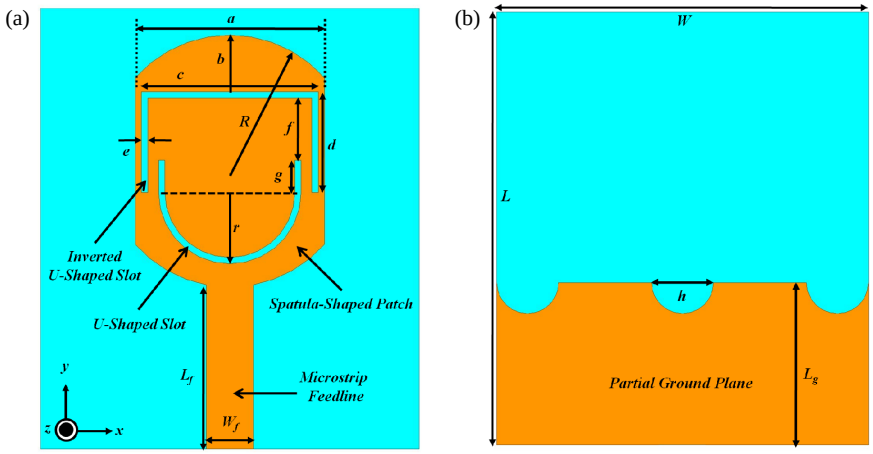

FIGURE 1. Single element monopole antenna design (a) top and (b) back views [$L = 28$, $W = 24$, $L_f = 10.45$, $W_f = 3$, $a = 12$, $b = 3.6$, $c = 11.2$, $d = 6.4$, $e = 0.4$, $f = 3.94$, $g = 2.06$, $h = 4$, $L_g = 10.5$, $R = 8$ and $r = 4.12$ (unit: mm)].

with very low isolation level of 13 dB was investigated in [18]. Later, in another approach, a 4-port transparent MIMO antenna created using metal mesh structure was studied for 3.2–11.2 GHz range [19]. It utilizes a parasitic decoupler to mitigate the inter-element coupling. Despite this, it could achieve a very low isolation level of 10 dB at lower frequencies and better than 20 dB at higher frequencies. Recently, an innovative MTM wall separating quad-port MIMO antenna elements was reported to significantly improve the isolation over 3.4–4 GHz and 4.7–5.1 GHz [11]. However, the adoption of MTM wall raises the overall profile of the antenna, making it more difficult to assemble due to its 3D form. An extensive literature survey demonstrates that it is very challenging to design a simple yet compact MIMO antenna that could provide extremely wide bandwidth and high inter-port isolation, while at the same time filtering out undesired interferences.

In this paper, a novel, compact super-wideband 4×4 MIMO antenna with very high inter-port isolation and dual-band interference shielding capability has been designed and successfully investigated for UWB and beyond. A substantial improvement in the isolation has been achieved by utilizing a swastik-shaped decoupling structure. The band extending from 2.63 to 18.44 GHz is above -10 dB reflection level except for two notch bands spanning over 3.38–3.90 GHz and 4.65–6.45 GHz; hence, the achieved bandwidth including notched frequencies is 150%. The diversity performance of the proposed MIMO antenna is evaluated by examining diversity metrics envelope correlation coefficient (ECC) and diversity gain (DG). Besides above, the investigation of surface current, radiation pattern, gain, and radiation efficiency demonstrates the potential use of the introduced MIMO antenna in X- and Ku-band satellite systems as well as sub-6 GHz 5G, WLAN, ISM, LTE, Wi-MAX, and UWB frequency bands.

2. DESIGN METHODOLOGY OF SINGLE ELEMENT ANTENNA

The top and bottom schematic configurations of the proposed UWB single element antenna featured with dual-notch band characteristic are shown in Figs. 1(a) and 1(b), respectively. It is implemented using a 1.6 mm thick FR4 dielectric substrate characterized by its dielectric constant of 4.4 and loss tangent of 0.02. The resonating element comprises a 50 Ω microstrip line fed-truncated circular patch (termed spatula-shaped patch hereafter), etched with a U and an inverted U-shaped slots. Further, defected partial ground plane has been employed to achieve improved impedance matching across the wide operating band [20]. This reduces the overall radiating patch area and ground plane; thereby resulting in miniaturized UWB monopole antenna. The intended antenna is designed and numerically investigated in full-wave 3D EM tool, i.e., Computer Simulation Technology (CST) Microwave Studio suite 2022. The optimized values of the design parameters denoted in Fig. 1 are listed in its caption.

The progressive evolution of the suggested antenna element is illustrated in Fig. 2, which shows the input reflection coefficient and respective design topology in the inset at different iterative stages. The design starts with a spatula-shape radiator having a semi-circular defected partial ground plane, called Antenna #1. It has been conceptualized by appropriately mod-

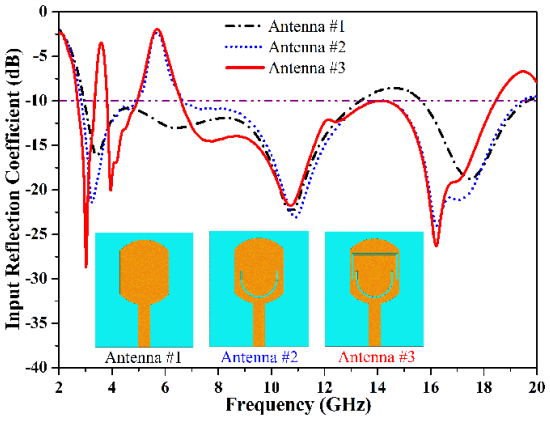

FIGURE 2. Design evolution of the proposed dual-notched super-wideband antenna: the structure at distinct iterative stages and their respective S_{11} (dB) curves.

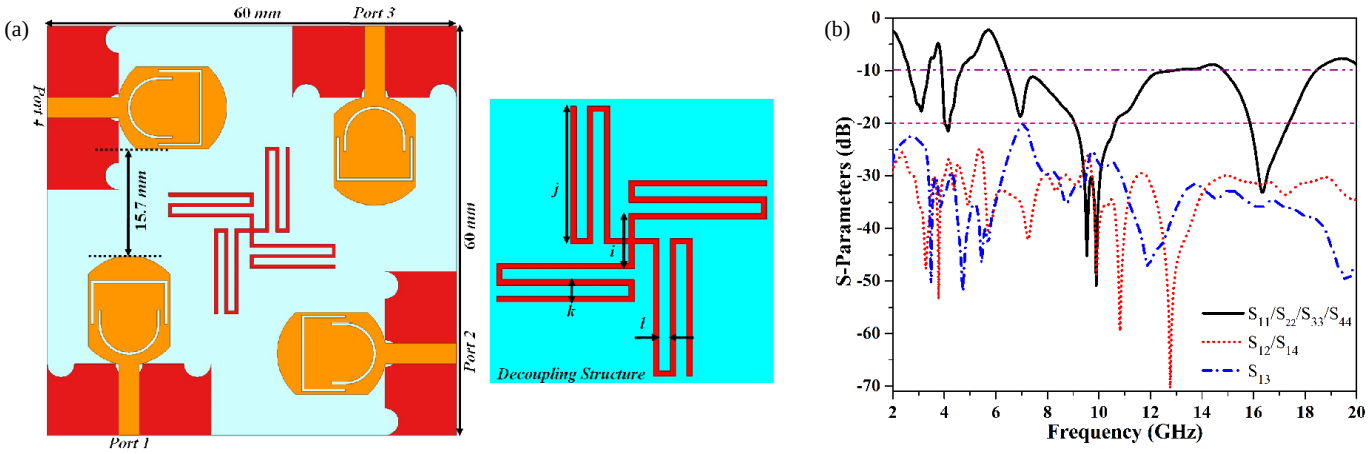

FIGURE 3. (a) Interactive schematic configuration and (b) S-parameters of the proposed 4-port MIMO antenna.

ifying the circular patch to obtain novelty in terms of antenna design. The dimensions were computed using well defined empirical relations mentioned in [21]. It can be observed that it provides UWB response covering 2.95–19.64 GHz with poor impedance matching across 13.35–15.64 GHz. In order to implement notch bands, slotting technique has been utilized. It is well established that the surface current can be attenuated or altered to some extent so that the antenna does not radiate energy outward by engraving slots in the antenna design [2]. Therefore, to suppress WLAN/ISM band, a U-shaped filter is imprinted in the radiator of Antenna #1, and it is denoted as Antenna #2. It is seen that Antenna #2 offers UWB response covering 2.84–19.45 GHz with a sharp notch band of 4.86–6.67 GHz centered at 5.69 GHz. Additionally, in order to filter out the Wi-MAX/LTE band, an inverted U-shaped slot is etched in the radiator, and this configuration is named Antenna #3. The resultant structure exhibits a UWB impedance matching spanning over 2.70–18.45 GHz (15.75 GHz) while rejecting 3.34–3.80 GHz (centered at 3.58 GHz) Wi-MAX/LTE band and 4.94–6.60 GHz (centered at 5.69 GHz) WLAN/ISM band. Note that dimensions of the slots were initially calculated using Equations (1)–(3) [17, 22] and later optimized for desired frequency response.

$$f_{3.58\,\text{GHz}} = \frac{3 \times 10^8}{2(c+2d)\sqrt{\varepsilon_{eff}}} \tag{1}$$

$$f_{5.69\,\text{GHz}} = \frac{3 \times 10^8}{2(\pi r+2g)\sqrt{\varepsilon_{eff}}} \tag{2}$$

$$\varepsilon_{eff} \approx (\varepsilon_r + 1)/2 \tag{3}$$

3. PLANAR 4×4 MIMO ANTENNA DESIGN

Afterwards, four identical single element antennas (Antenna #3) described above are arranged systematically in the orthogonal fashion on the same substrate to form MIMO configuration with the aim to achieve polarization diversity and high inter-port isolation. It is important to note that the two radiating elements are separated by 15.7 mm (0.13λ), where λ is the wavelength evaluated at the lowest operating frequency of 2.63 GHz. A decoupling structure is strategically placed in the center of the ground plane to further enhance the mutual coupling. It comprises a swastik-shaped structure with its arms extended in the form of meander lines. The 4×4 planar MIMO antenna has an overall footprint of 60 mm $\times$ 60 mm ($0.52\lambda \times 0.52\lambda$), which is compact as compared to the ones reported in [8, 23, 24]. Fig. 3(a) visually illustrates the transparent top and bottom structural details of the suggested 4-port MIMO antenna. The design parameter values of the decoupling network for the enhanced performance are: $i = 5$ mm, $j = 12$ mm, $k = 2$ mm, and $l = 1$ mm. The simulated S-parameters of the conceived MIMO antenna are depicted in Fig. 3(b).

It is clear that it operates as a UWB antenna with an operational bandwidth of 15.81 GHz extended over the frequency range of 2.63–18.44 GHz with dual-notched characteristics at 3.75 GHz and 5.70 GHz. These notch-bands serve to filter out any potential interference arising from WLAN/ISM (3.38–3.90 GHz) and Wi-MAX/LTE (4.65–6.45 GHz) bands. A bit of mismatch is observed between the single element and MIMO antennas which are attributed to interrelations of the four an-

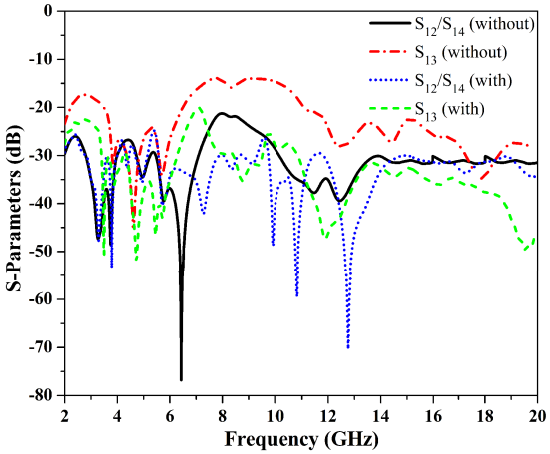

FIGURE 4. Mutual coupling among the 4-ports of the suggested MIMO antenna without and with decoupling structure.

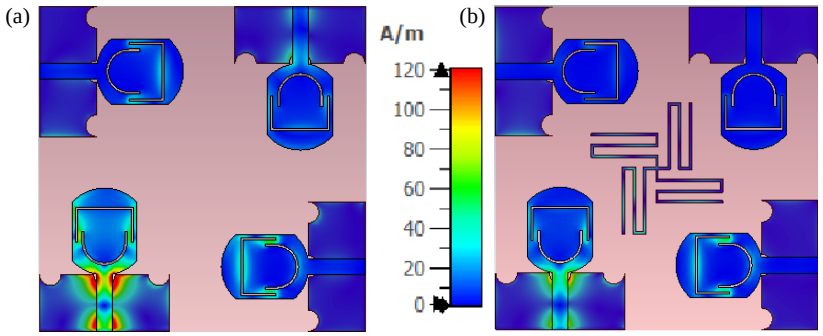

FIGURE 5. Surface current distribution at 8.73 GHz over the antenna (a) without and (b) with decoupling structure.

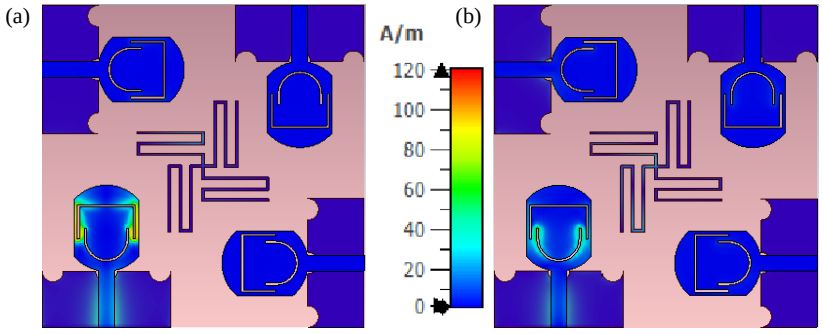

FIGURE 6. Surface current distribution at the notched frequencies: (a) 3.75 GHz and (b) 5.70 GHz.

tenna elements. Owing to the symmetrical antenna topology, Port #1, Port #2, Port #3, and Port #4 all have identical reflection coefficients. The isolation between Port #1 and Port #3 (diagonal elements) is found to be 20 dB due to small amount of EM coupling from the radiating edges of the antenna elements. However, an enhanced isolation of 25 dB between Port #1 & Port #2 and Port #1 & Port #4 (orthogonal elements) is noted due to almost negligible electromagnetic (EM) coupling between radiating and non-radiating edges of the antenna elements.

To demonstrate the proposition of decoupling structure, the proposed MIMO antenna has been investigated for inter-port isolation in relation to the absence and presence of decoupling structure. The corresponding transmission coefficients are compared in Fig. 4. It is discovered from Fig. 4 that the inclusion of the decoupling structure has improved isolation among the orthogonal and diagonal elements by around 3.5 dB (from 21.5 dB to 25 dB) and 6 dB (from 14 dB to 20 dB), respectively. Notably, the two reflection coefficients are not shown here for the sake of brevity because they are unaltered.

In addition, the surface current density over the antenna without and with a decoupling structure, taken at 8.73 GHz with Port #1 excited, augments the effectiveness of the decoupling structure, as demonstrated in Fig. 5. Without the decoupling structure, the nearby antenna elements exhibit high current coupling, as seen in Fig. 5(a). On the contrary, Fig. 5(b) shows that when a decoupling structure is added into the MIMO design, a considerable amounts of currents are induced over it, and the current on the neighbouring antenna elements decreases drastically. Consequently, the interference from the adjacent antennas is reduced, resulting in improved overall performance of the put forth MIMO system.

Further, the distribution of surface current density is examined at the notch frequencies of 3.75 GHz and 5.70 GHz to ensure the adequate isolation among different ports of the intended 4×4 MIMO design. Notably, Port #1 was excited while all the other ports were termination by a load of 50 Ω in this study. It is clear from Fig. 6 that the surface current is predominantly concentrated on inverted U- and U-shaped slots at 3.75 GHz and 5.70 GHz correspondingly. It indicates a large impedance mismatch, with almost all the incident signals being reflected backwards, resulting in dual-band filtering functionality. In addition, no EM coupling is seen with the neighbouring antenna elements which demonstrate exceptional diversity performance. The above analysis also corroborates the findings presented in Section 2.

4. EXPERIMENTAL RESULTS AND DISCUSSION

4.1. Reflection Coefficient and Isolation

Finally, a prototype of the realized super-wideband MIMO antenna is developed to validate its practicality. Figs. 7(a)–(b) show photographs of the fabricated prototype. The performance testing was conducted by utilizing Anritsu S820E handheld vector network analyzer (VNA), as seen in Fig. 7(c). Fig. 7(d) depicts the radiation pattern and gain measurement setup, which consists of a broadband horn antenna and constructed sample mounted on a turntable, both inside an anechoic

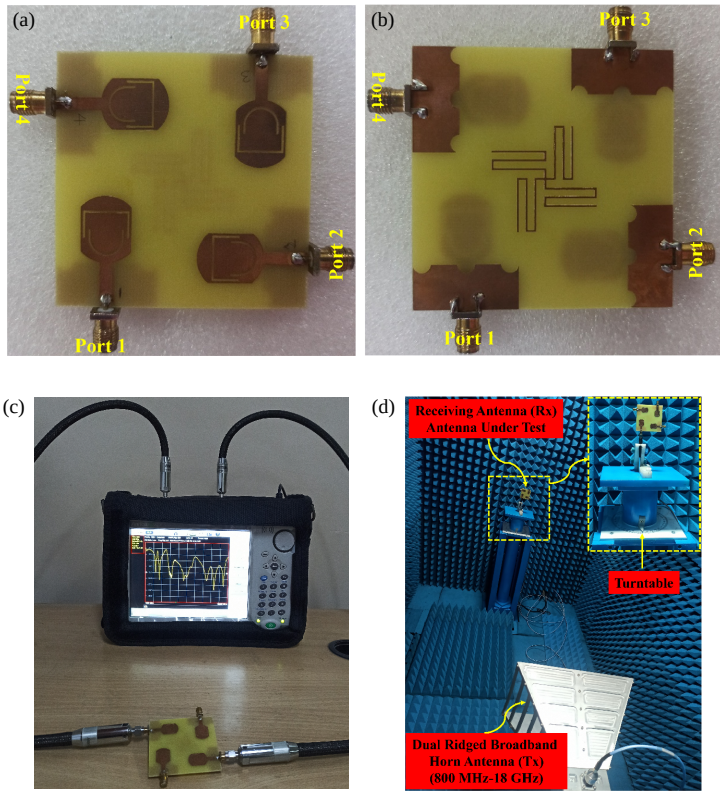

FIGURE 7. (a) Top view, (b) bottom view of the fabricated prototype of the 4×4 UWB MIMO antenna, (c) S-parameter measurement setup, and (d) measurement setup for far-field measurement inside an anechoic chamber.

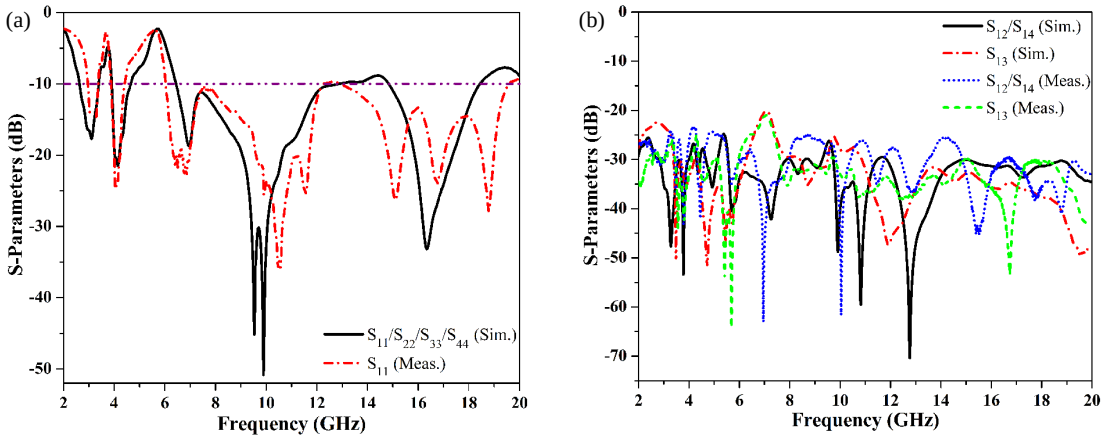

FIGURE 8. Simulated and measured (a) reflection coefficients and (b) transmission coefficients.

chamber and coupled to an external VNA. A comparison between the simulated and measured S-parameters is presented in Fig. 8. It can be seen that there is an excellent correlation between the two results in terms of notched-band frequencies and inter-port isolation levels, confirming conceptual projections of the antenna's performance. However, a slight deviation in the resonant peaks and operational bandwidth is noticed, which is subjected to manufacturing error and measurement inaccuracies. It is worth noting that owing to structural symmetry, the input reflection coefficients of all the ports are almost similar with trivial variations in the notched-band frequencies; hence, only measured S_{11} is furnished in Fig. 8(a) for clear visualization. In addition, the isolation curves obtained from measurement and simulation are displayed in Fig. 8(b). The measured transmission coefficients illustrate that the isolation level at S_{12} or S_{14} is better than 23 dB while the isolation level at S_{13} is greater than 20.5 dB. The summary of the simulated and measured results is presented in Table 1 for better and quick grasp.

4.2. Radiation Patterns, Gain, and Radiation Efficiency

Figure 9 illustrates the simulated and measured 2D radiation patterns of the reported antenna plotted in two principal planes

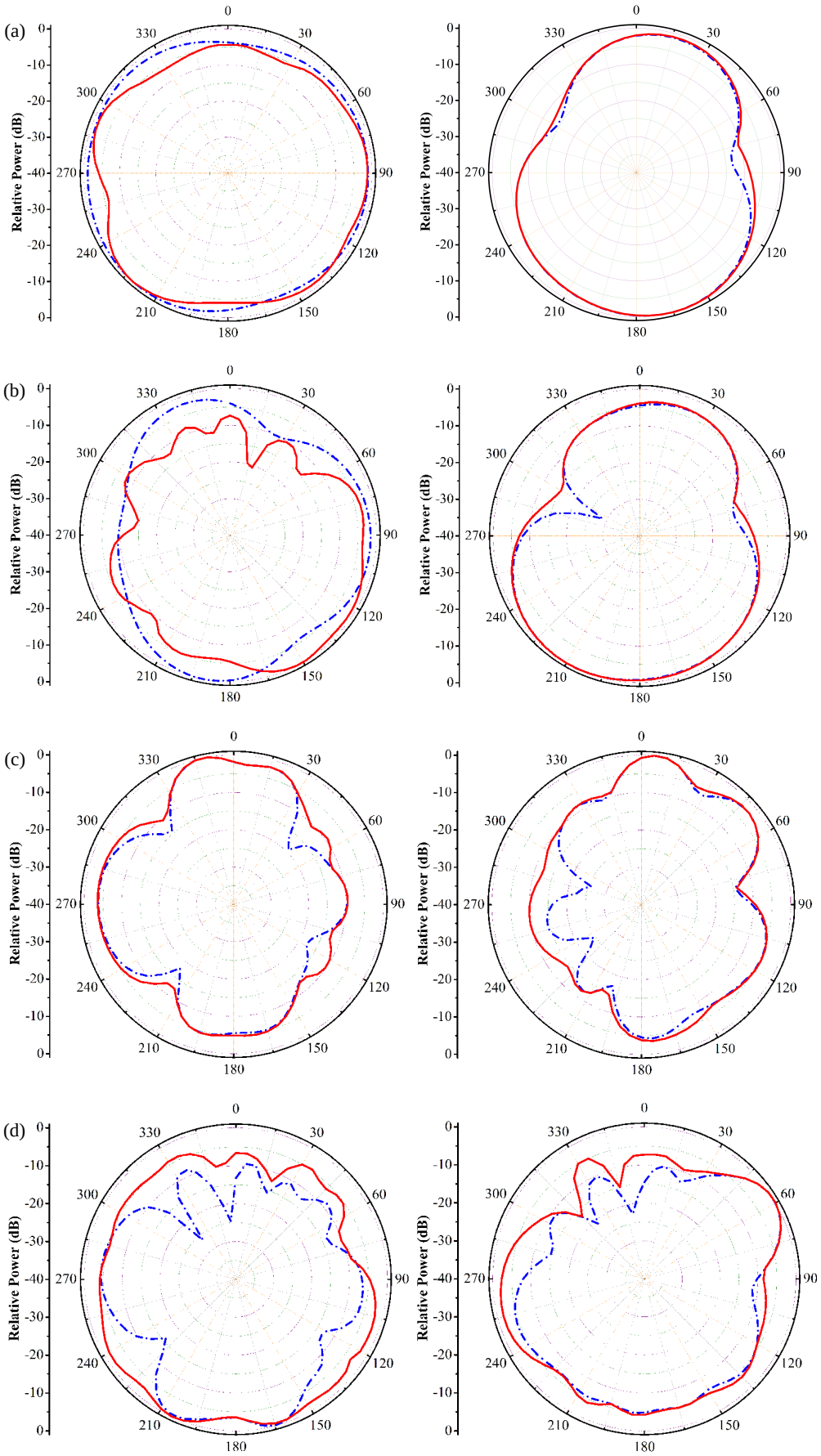

FIGURE 9. Simulated (dash dot in blue) and measured (sold in red) normalized radiation patterns of the introduced super-wideband 4-port MIMO antenna in *xz* [left] and *yz* [right] planes. (a) 3.11 GHz, (b) 4.14 GHz, (c) 9.89 GHz, (d) 16.33 GHz.

TABLE 1. Comparison between the simulated results and measured counterparts.

Characteristics	Operating Band (GHz)	Notch Bandwidth, Centre Frequency (GHz)	Isolation Between S_{12}/S_{14} (dB)	Isolation Between S_{13} (dB)
Simulated	2.63–18.44	3.38–3.90, 3.75 4.65–6.45, 5.70	25	20
Measured	2.95–19.58	3.37–3.87, 3.68 4.40–6.03, 5.55	23	20.5

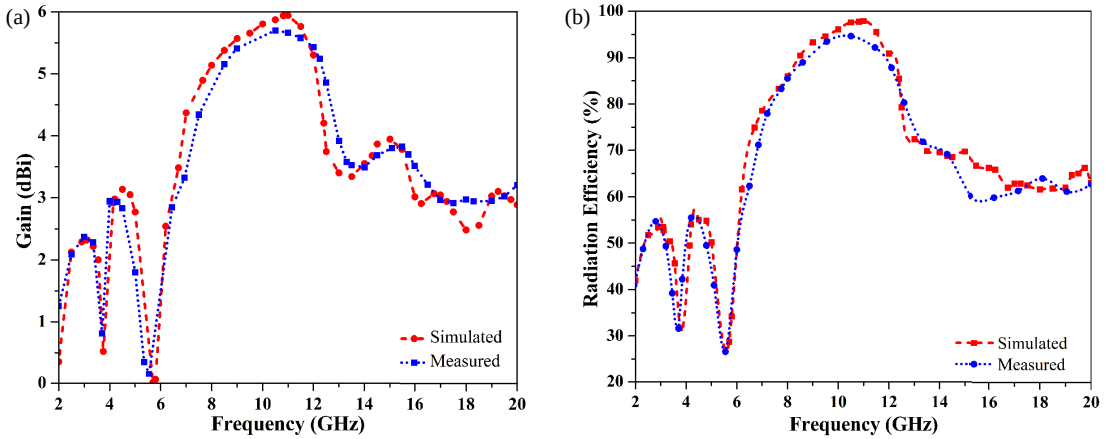

FIGURE 10. Simulated and measured (a) gains and (b) radiation efficiencies of the recommended MIMO antenna.

when Port #1 is excited at 3.11 GHz, 4.14 GHz, 9.89 GHz, and 16.33 GHz. The dash dot line in blue and solid line in red denote simulated and measured radiation patterns of the antenna, respectively. It is evident that the patterns are rather stable at lower frequencies, but some irregularity is noticed around 16.33 GHz. Moreover, the measured patterns agree well with that of simulated ones. However, a small discrepancy is seen between the two radiations, especially at higher frequencies, which could be attributed to fabrication flaws and measurement limitations.

Next, the gain along with radiation efficiency of the presented MIMO structure is illustrated in Fig. 10. The antenna is capable to offer a maximum of 5.94 dBi simulated gain, with the lowest value being 0.01 dBi in the notched bands whereas the measured gain varies from 0.06 to 5.88 dBi across the studied frequency range. Furthermore, the simulated radiation efficiency ranges between 41.94% and 97.88% in the working band, except for notched frequencies. However, it is less than 50% in both notched bands, with a minimum of 28.76% at 5.70 GHz. The measured radiation efficiency attains maximum and minimum values of 94.65% and 26.59% at 10.5 GHz and 5.55 GHz, respectively.

4.3. MIMO Diversity Metrics Analysis

For the practical implementation, the diversity performance of a MIMO antenna is quantified in terms of envelope correlation coefficient (ECC) and diversity gain (DG). ECC indicates the degree of correlation between the signals received at the adjacent antenna elements [1]. Lower value of ECC is sought after for better signal quality and system reliability. Mathematically, it is computed from S-parameters by using Equation (4) [1]. It is clear from Fig. 11(a) that over the whole frequency range under investigation, the ECC of the proposed MIMO design is seen to be < 0.012, which is substantially within the allowable limit of 0.5.

$$\mathrm{ECC} = \frac{\left|S_{11}^{*}S_{12} + S_{21}^{*}S_{22}\right|^{2}}{\left(1 - \left|S_{11}\right|^{2} - \left|S_{21}\right|^{2}\right)\left(1 - \left|S_{22}\right|^{2} - \left|S_{12}\right|^{2}\right)} \quad (4)$$

Diversity gain (DG) is another metric used to assess the MIMO antenna's stability and efficacy. Ideally, DG must be quite high, nearly close to 10 dB. DG can be calculated by using ECC value as per Equation (5) [1].

$$\mathrm{DG} = 10\sqrt{1 - \mathrm{ECC}^{2}} \quad (5)$$

Figure 11(b) denotes that both simulated and measured values of DG are above 9.995 dB over the operational frequency range, with somewhat reduced diversity performance within notch bands. Such favourable numbers of ECC and DG verify that the adjacent ports are uncorrelated, and the intended MIMO antenna is well suited for UWB, X, and Ku band applications.

5. COMPARISON WITH STATE-OF-ART

Finally, the suggested MIMO antenna is comprehensively compared with the recently reported 4-port MIMO antennas with

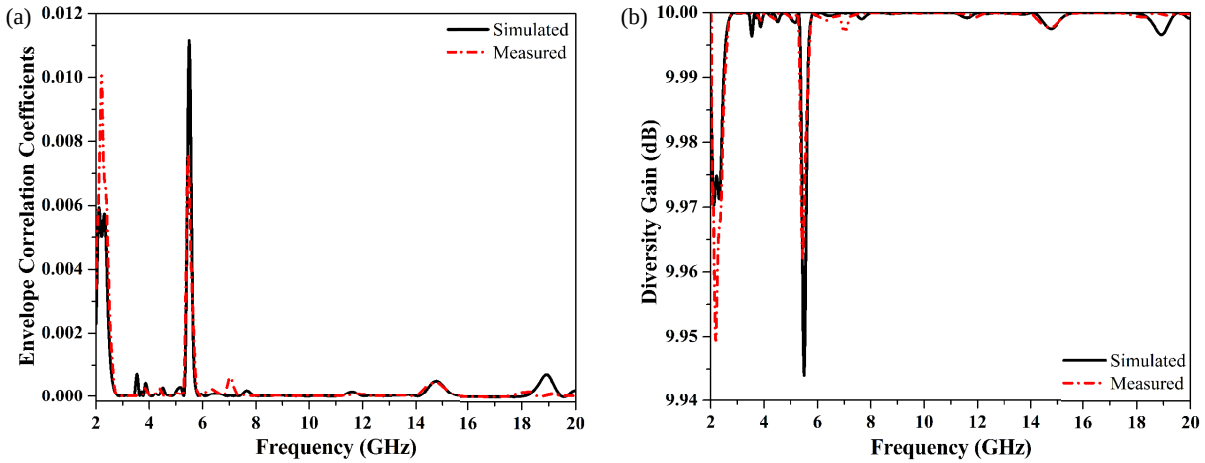

FIGURE 11. Simulated and measured (a) ECCs and (b) DGs of the proposed 4×4 MIMO antenna.

TABLE 2. Comparative performance evaluation of the proposed 4×4 MIMO antenna with present state-of-art.

Ref.	Dimensions L × W × H, mm³ (L × W × H, λ³)	Operational Band (GHz)	Notch Band (GHz)	Notch Method	Isolation (dB)	Isolation Improvement Technique	Gain (dBi)	ECC
[5]	50 × 50 × 1.6 (0.33 × 0.33 × 0.01)	2-12	4.91-6.41	L-Shaped Stub Connected in Partial Ground	> 17	Slot in Orthogonal Radiators	3.3	< 0.45
[8]	56 × 68 × 0.235 (0.72 × 0.88 × 0.0025)	3.89-17.09	None	Not Applicable	> 15	Modified Plus-Shaped Slot Separating CPW-Fed Elements	6.8	< 0.02
[13]	34 × 34 × 1.6 (0.28 × 0.28 × 0.013)	2.5-12	3.3-3.9 5-6 7.4-8.5	L & C-Shaped Slots, and EBG	> 15	Parasitic Strips Connected to Ground through vias	5.5	< 0.05
[16]	45 × 55 × 1 (0.47 × 0.58 × 0.01)	3.19-9.30	None	Not Applicable	> 20	Slots in Substrate	2.49	< 0.02
[18]	56 × 56 × 1.6 (0.42 × 0.52 × 0.014)	2.8-15.2	None	Not Applicable	> 20	Orthogonal Placement on Top and Bottom	6.6	< 0.01
[22]	40 × 40 × 0.05 (0.51 × 0.51 × 0.00063)	3.82-15.9	None	Not Applicable	> 17 > 20	L-Shaped Strips Connected around Radiator	6.33	< 0.005
[23]	60 × 60 × 1.52 (0.60 × 0.60 × 0.015)	3-12.8	5.25-5.85	EBG	> 21	Parasitic Decoupler	6.94	< 0.001
[24]	58 × 58 × 1.6 (0.55 × 0.55 × 0.015)	2.84-15.88	None	Not Applicable	> 16	Slot in Surface	6.35	< 0.07
[25]	56 × 41 × 1.6 (0.63 × 0.46 × 0.018)	3.4-11.8	None	Not Applicable	> 20	Square Slotted Decoupling Structure	6.23	< 0.006
[26]	56 × 56 × 0.787 (0.68 × 0.68 × 0.009)	3.65-13.97	None	Not Applicable	> 21.7	Windmill Like Decoupling Structure	7.2	< 0.0012
[27]	40 × 40 × 0.8 (0.56 × 0.56 × 0.011)	4.2-8.2	None	Not Applicable	> 23	Sinusoidal Decoupling Structure	7.9	< 0.0005
This Work	**60 × 60 × 1.6 (0.52 × 0.52 × 0.014)**	**2.63-18.44**	**3.38-3.90 4.65-6.45**	**U and Inverted U-Shaped Slots**	**> 20 > 25**	**Swastik Shaped Decoupling Structure**	**5.94**	**< 0.012**

respect to some key technical points, and the outcome is summarized in Table 2. It is obvious that the intended MIMO antenna yields the largest impedance bandwidth amongst all the designs. Moreover, it occupies less circuit area except for MIMO designs [5, 13, 16, 18, 22]. Nevertheless, the design in [5] offers single-band rejection capability and low inter-element isolation level. In addition, the antenna in [13] provides triple-band notch feature, but the implementation of EBG structure is complicated due to involved via processes. Also, it achieves very low isolation level, even after utilizing parasitic strips connected to ground through vias. Further, the antennas in [16, 18, 22] do not possess notched characteristics and have complex structures. Taking into account the aperture area and substrates used, the proposed MIMO antenna exhibits comparable or better performance in terms of peak gain and diversity.

6. CONCLUSION

A 4-port MIMO antenna with dual-notched feature is fabricated on a cost-effective FR4 substrate and tested to confirm the theoretical conceptualizations. It yields a super-wideband impedance bandwidth of 15.81 GHz with a relative bandwidth of 150% spanning 2.63–18.44 GHz range with the ability to efficiently reject two interfering bands extended over 3.38–3.90 GHz and 4.65–6.45 GHz. Besides this, it outperforms many MIMO designs that rely on bulky or fabrication-intensive methods like MTM walls or parasitic vias, with high measured inter-port isolation of 20.5 dB (diagonal elements) and 23 dB (adjacent elements). It is observed that the orthogonal antenna arrangement and decoupling structure in the centre of the ground plane are responsible for such high inter-port isolation in the recommended MIMO device. Moreover, the proposed decoupling structure enhances peak radiation efficiency from 91.16% to 97.88%, yielding an improvement of 7.37%. In addition, the suggested MIMO antenna is capable to achieve radiation efficiency and gain as high as 97.88% and 5.94 dBi, respectively with consistent radiation pattern in principal planes. The diversity performance metrics, ECC < 0.012 and DG > 9.995 dB, ensure low signal correlation and high reliability in multipath environments. The peculiar properties of the proposed antenna make it well suited for the smart devices operating in sub-6 GHz 5G, WLAN, ISM, LTE, Wi-MAX, UWB frequency bands, and X- & Ku-band satellite systems. The integration of tunable component (e.g., PIN diode, varactor diode, and micro-electromechanical switches (MEMSs)) into the design to dynamically adjust notch frequencies is identified as possible future research extension of this work. It will enable adaptive interference mitigation for evolving wireless standards like 6G and beyond.

REFERENCES

[1] Sharma, M., V. Dhasarathan, S. K. Patel, and T. K. Nguyen, "An ultra-compact four-port 4×4 superwideband MIMO antenna including mitigation of dual notched bands characteristics designed for wireless network applications," *AEU — International Journal of Electronics and Communications*, Vol. 123, 153332, 2020.

[2] Yang, W., X. Zhao, Z. Guo, H. Sun, and E. J. W. List-Kratochvil, "A compact tri-notched flexible UWB antenna based on an inkjet-printable and plasma-activated silver nano ink," *Scientific Reports*, Vol. 14, No. 1, 11407, 2024.

[3] Jaglan, N., S. D. Gupta, E. Thakur, D. Kumar, B. K. Kanaujia, and S. Srivastava, "Triple band notched mushroom and uniplanar EBG structures based UWB MIMO/diversity antenna with enhanced wide band isolation," *AEU — International Journal of Electronics and Communications*, Vol. 90, 36–44, 2018.

[4] Sediq, H. T., "Miniaturized MIMO antenna design based on octagonal-shaped SRR metamaterial for UWB applications," *AEU — International Journal of Electronics and Communications*, Vol. 172, 154946, 2023.

[5] Khan, M. S., A. Iftikhar, R. M. Shubair, A. D. Capobianco, B. D. Braaten, and D. E. Anagnostou, "A four element, planar, compact UWB MIMO antenna with WLAN band rejection capabilities," *Microwave and Optical Technology Letters*, Vol. 62, No. 10, 3124–3131, 2020.

[6] Wang, B., D. Yang, and K. Sun, "Design and analysis of a compact omnidirectional UWB slot antenna," *Microwave and Optical Technology Letters*, Vol. 61, No. 8, 1917–1923, 2019.

[7] Kaiser, T., F. Zheng, and E. Dimitrov, "An overview of ultra-wide-band systems with MIMO," *Proceedings of the IEEE*, Vol. 97, No. 2, 285–312, 2009.

[8] Desai, A., J. Kulkarni, M. M. Kamruzzaman, S. Hubálovský, H.-T. Hsu, and A. A. Ibrahim, "Interconnected CPW fed flexible 4-port MIMO antenna for UWB, X, and Ku band applications," *IEEE Access*, Vol. 10, 57 641–57 654, 2022.

[9] Jaglan, N., S. D. Gupta, B. K. Kanaujia, and M. S. Sharawi, "10 element sub-6-GHz multi-band double-T based MIMO antenna system for 5G smartphones," *IEEE Access*, Vol. 9, 118 662–118 672, 2021.

[10] Jaglan, N., S. D. Gupta, and M. S. Sharawi, "18 element massive MIMO/diversity 5G smartphones antenna design for sub-6 GHz LTE bands 42/43 applications," *IEEE Open Journal of Antennas and Propagation*, Vol. 2, 533–545, 2021.

[11] Wang, H., Q. Zheng, Q. Li, and X.-X. Yang, "Isolation improvement and bandwidth enhancement of dual-band MIMO antenna based on metamaterial wall," *IEEE Antennas and Wireless Propagation Letters*, Vol. 24, No. 5, 1144–1148, 2025.

[12] Kayabasi, A., A. Toktas, E. Yigit, and K. Sabanci, "Triangular quad-port multi-polarized UWB MIMO antenna with enhanced isolation using neutralization ring," *AEU — International Journal of Electronics and Communications*, Vol. 85, 47–53, 2018.

[13] Chen, Z., W. Zhou, and J. Hong, "A miniaturized MIMO antenna with triple band-notched characteristics for UWB applications," *IEEE Access*, Vol. 9, 63 646–63 655, 2021.

[14] Alibakhshikenari, M., B. S. Virdee, C. H. See, R. Abd-Alhameed, A. H. Ali, F. Falcone, and E. Limiti, "Study on isolation improvement between closely-packed patch antenna arrays based on fractal metamaterial electromagnetic bandgap structures," *IET Microwaves, Antennas & Propagation*, Vol. 12, No. 14, 2241–2247, 2018.

[15] Hassan, M. M., M. Rasool, M. U. Asghar, Z. Zahid, A. A. Khan, I. Rashid, A. Rauf, and F. A. Bhatti, "A novel UWB MIMO antenna array with band notch characteristics using parasitic decoupler," *Journal of Electromagnetic Waves and Applications*, Vol. 34, No. 9, 1225–1238, 2020.

[16] Desai, A., H.-T. Hsu, B. M. Yousef, A. M. Ameen, Y.-F. Tsao, and A. A. Ibrahim, "UWB connected ground transparent 4-port flexible MIMO antenna for IoT applications," *IEEE Internet of Things Journal*, Vol. 11, No. 7, 12 475–12 484, 2024.

[17] Modak, S., T. Khan, T. A. Denidni, and Y. M. M. Antar, "Miniaturized self-isolated UWB MIMO planar/cuboidal antenna with dual X-band interference rejection," *AEU — International Journal of Electronics and Communications*, Vol. 143, 154020, 2022.

[18] Addepalli, T., J. B. Kamili, S. Boddu, R. Manda, A. Nella, and B. K. Kumar, "A 4-element crescent shaped two-sided MIMO antenna for UWB, X and Ku band wireless applications," *Wireless Networks*, Vol. 29, No. 8, 3333–3348, 2023.

[19] Yao, Y., Y. Shao, J. Zhang, and J. Zhang, "A transparent antenna using metal mesh for UWB MIMO applications," *IEEE Transactions on Antennas and Propagation*, Vol. 71, No. 5, 3836–3844, 2023.

[20] Durukan, T. and Y. Altuncu, "A compact 4×4 reconfigurable MIMO antenna design with adjustable suppression of certain frequency bands within the UWB frequency range," *AEU — International Journal of Electronics and Communications*, Vol. 170, 154848, 2023.

[21] Balanis, C. A., *Advanced Engineering Electromagnetics*, John Wiley & Sons, New York, 1989.

[22] Rajesh, G. and R. Poonkuzhali, "Design and analysis of CPW fed ultrathin flexible MIMO antenna for UWB and X-band applications," *IEEE Access*, Vol. 12, 96 704–96 717, 2024.

[23] Abbas, A., N. Hussain, M. A. Sufian, J. Jung, S. M. Park, and N. Kim, "Isolation and gain improvement of a rectangular notch UWB-MIMO antenna," *Sensors*, Vol. 22, No. 4, 1460, 2022.

[24] Balaji, V. R., T. Addepalli, A. Desai, A. Nella, and T. K. Nguyen, "An inverted L-strip loaded ground with hollow semi-hexagonal four-element polarization diversity UWB-MIMO antenna," *Transactions on Emerging Telecommunications Technologies*, Vol. 33, No. 1, e4381, 2022.

[25] Jhunjhunwala, V. K., P. Kumar, A. P. Parameswaran, P. R. Mane, O. P. Kumar, T. Ali, S. Pathan, S. Vincent, and P. Kumar, "A four port flexible UWB MIMO antenna with enhanced isolation for wearable applications," *Results in Engineering*, Vol. 24, 103147, 2024.

[26] Li, C., Z. Wang, W. Nie, and M. Yang, "A four port ultra-wideband MIMO antenna with windmill shaped decoupling structure and Olympic five ring patch," *Progress In Electromagnetics Research C*, Vol. 155, 255–264, 2025.

[27] Pandurangan, D. and N. Mishra, "Circularly polarized four-element wideband MIMO antenna for C-band applications using sinusoidal decoupling structure for isolation and axial ratio enhancement," *Results in Engineering*, Vol. 26, 105301, 2025.